International Journal of Solids and Structures 49 (2012) 338–343

Contents lists available at SciVerse ScienceDirect

International Journal of Solids and Structures

journal homepage: www.elsevier.com/locate/ijsolstr

A new efficient numerical method for contact mechanics of rough surfaces

C. Putignano, L. Afferrante *, G. Carbone, G. Demelio

DIMeG-Politecnico di Bari, v.le Japigia 182, 70126 Bari, Italy

ARTICLE INFO

Article history:
Received 19 January 2011
Received in revised form 7 July 2011
Available online 14 October 2011

Keywords:
Rough surfaces
Adhesionless contact
Green's function

ABSTRACT

In this work, a numerical method has been developed to investigate the adhesionless contact mechanics between rough surfaces. To solve the elastic problem a boundary elements approach is used with self-equilibrated square elements. The domain of integration is discretized developing an "intelligent" adaptive mesh and obtaining a considerable memory saving. The numerical convergence of the method has been verified by comparing the results with the Hertzian solution and by checking the stress probability distribution at the contact interface. The methodology has been then utilized to analyse the contact between an elastic flat substrate and a periodic numerically generated self-affine fractal rigid surface. The fractal surface has been generated by employing spectral methods. The results of our investigation supports the findings of some analytical theories (Persson, 2001) and numerical findings (Yang et al., 2006; Hyun et al., 2004; Carbone and Bottiglione, 2008; Campana and Muser, 2007) in terms of linearity between contact area and load and stress probability distributions.

1. Introduction

Contact between rough surfaces occurs widely in engineering systems: the micromechanical characteristics of the contact process have great effect on technologically important cases such as friction, contact stiffness and electrical contact resistance. Recently, these topics have gained an increasing interest as an effect of the wide effort to realize smaller and smaller mechanical and electrical devices down to the micro- and nano-scales (Sundararajan and Bhushan, 2001) and to realize newly conceived bio-inspired adhesives (Geim et al., 2003). As an example, in fact, in the case of microelectromechanical systems (MEMS), large contact areas produce large adhesion forces with the consequent adhesion of the moving parts and, then, the global failure of the system.

There are lots of approaches to this problems, dealing with the contact of real random rough surfaces. Greenwood and Williamson introduced asperity-based models (Greenwood and Williamson, 1966; Greenwood et al., 2011), initially based on a set of identical asperities distributed according to a Gaussian or exponential height distribution: in this analytical model, every asperity is assimilated to a Hertzian punch. Later models have used random process theory to make the asperity curvature depending on their heights or have resorted to an apparently different approach that uses fractal theories to recognize more directly the multiscale nature of most real surface (Greenwood, 2006). Although they achieved result being worth of practical interest, these multi-asperity models have a significant lack: they do not take into account interactions between microcontacts. This problem is clearly heavier when we study situations approaching full contact, i.e. when the contact spot separation is of comparable size with the spot size itself. To overcome these question, Persson (2001) has proposed a new model, which gives the exact solution for the case of full contact, and an approximate solution in partial contact situations.

In this work, a numerical approach is developed to evaluate the elastic contact solution between a rigid rough surface and an linear elastic half-space. This approach makes use of a boundary element method based on a non-uniform adaptive meshing scheme and on a "double-check" iterative process.

2. Mathematical formulation

The geometry of the problem under investigation is shown in Fig. 1, where the adhesionless contact between a periodic numerically generated isotropic randomly rough rigid surface and a linear elastic half-space is shown. In particular, it is shown that the elastic displacement of the half-space is the sum of two terms the first is just equal to the average displacement $\mathbf{u}_m(z)$ the second $\mathbf{v}(\mathbf{x},z) = \mathbf{u}(\mathbf{x},z) - \mathbf{u}_m(z)$, where $\mathbf{x}$ is the in-plane position vector, is just the additional displacement caused by the asperities induced deformation of the rough surfaces. Focusing only at the interface $z = 0$ we observe that the maximum value of the normal displacement $v(\mathbf{x}) = v_z(\mathbf{x}, z = 0)$ is just the penetration Δ of the rough surface into the half-space.

* Corresponding author. Tel.: +39 080 596 3793.
E-mail address: luciano@poliba.it (L. Afferrante).

0020-7683/$ - see front matter © 2011 Elsevier Ltd. All rights reserved.
doi:10.1016/j.ijsolstr.2011.10.009

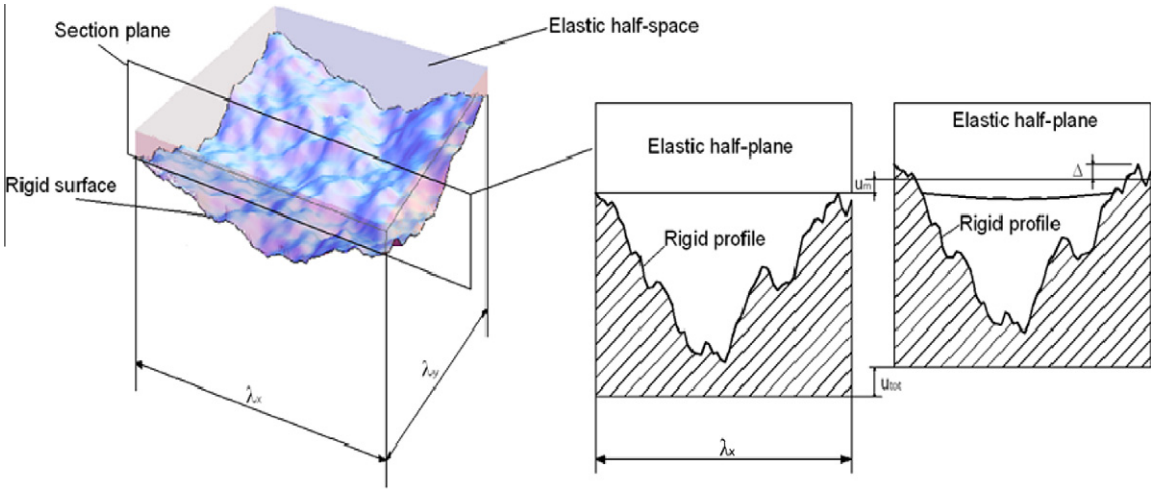

Fig. 1. An elastic half-space in adhesionless contact with a rough periodic rigid surface.

We assume that the roughness $h(\mathbf{x})$ (i.e. the distance from the mean plane) of the rigid surface is described by a self-affine geometry, that has been numerically generated by employing spectral methods. The fractal dimension of the surface is determined by the Hurst exponent H through the relation $D_f = 3 - H$. The power spectral density (PSD) of self-affine fractal surfaces is simply related to the wave vector $\mathbf{q} \equiv (q_x, q_y)$ where through a power law relation, that for isotropic surface is

$$C(q) = C_0 \left(\frac{q}{q_0}\right)^{-2(1+H)} \tag{1}$$

where $q = |\mathbf{q}|$ and q_0 is the roll-off wave vector. In order to carry out the numerical calculations, we have utilized a periodic surface with Fourier components up to the value $q_1 = Nq_0$, where N is the number of wavelengths. More details about the generation of the fractal surface are given in Appendix A.

To avoid border effects a periodic formulation is adopted by considering a periodic domain constituted of square cells $D = [(-\lambda/2, \lambda/2) \times (-\lambda/2, \lambda/2)]$. In the framework of linear elasticity the elastic displacement field at the interface can be written in terms of the interfacial normal stress $\sigma(\mathbf{x}) = \sigma_{zz}(\mathbf{x}, z = 0)$ as (Carbone and Mangialardi, 2004; Carbone and Mangialardi, 2008)

$$u_z(\mathbf{x}) = \int_D d^2s G(\mathbf{x} - \mathbf{s})\sigma(\mathbf{s}) \quad \mathbf{x} \in D \tag{2}$$

where $G(\mathbf{x})$ is the Green function. However, we observe that, in the case of infinite half-space under periodic load conditions, the mean displacement u_m of the elastic body at the interface is unbounded, and therefore only the term $v(\mathbf{x}) = u_z(\mathbf{x}) - u_m$ is finite. Since our focus is just on $v(\mathbf{x})$ we need to reformulate the problem in such a way that only the quantities $\sigma(\mathbf{x})$ and the $v(\mathbf{x})$ appears. To this end from Eq. (2) we obtain $u_m = \int_D d^2s G_m \sigma(\mathbf{s})$ with $G_m = \lambda^{-2} \int_D d^2x G(\mathbf{x})$, so that we can write

$$v(\mathbf{x}) = \int_D d^2s \mathcal{L}(\mathbf{x} - \mathbf{s})\sigma(\mathbf{s}) \quad \mathbf{x} \in D \tag{3}$$

where $\mathcal{L}(\mathbf{x}) = G(\mathbf{x}) - G_m$, is the elastic displacement at the interface $u_z(\mathbf{x})$ caused by a periodically applied self-balanced normal stress distribution $\sigma(\mathbf{x}) = \delta(\mathbf{x}) - \lambda^{-2}$, as it can be easily verified substituting in Eq. (2) such stress distribution: $u_z(\mathbf{x}) = \int_D d^2s G(\mathbf{x} - \mathbf{s})[\delta(\mathbf{s}) - \lambda^{-2}] = G(\mathbf{x}) - G_m = \mathcal{L}(\mathbf{x})$. To solve the contact problem we control penetration depth Δ and discretize the domain D in small squares of non uniform size. The unknown stress acting on each single square is assumed to be uniformly distributed on it. The discretized version of Eq. (3) becomes

$$v_i = L_{ij}\sigma_j \tag{4}$$

where v_i is the central displacement of each square, σ_i is the uniform stress on the square and L_{ij} is the elastic response matrix (i.e. the matrix associated to the discretized version of Eq. (3)), caused by the self-balanced applied load shown in Fig. 2.

L_{ij} can be calculated by recalling the Love solution (see Johnson, 1985) which gives the elastic displacement due to a uniform pressure acting on a rectangular area, and summing up the contribution of each elementary cell D to take into account the periodicity of the problem. Thus $L_{ij} = l_{ij} - l_m$, where

$$\begin{aligned} l_{ij} = \frac{1-\nu^2}{\pi E} \sum_{k=-\infty}^{+\infty} \sum_{h=-\infty}^{+\infty} & \times \left\{ (\xi_{ij} + d_j) \ln \left(\frac{(\eta_{ij} + d_j) + [(\xi_{ij} + d_j)^2 + (\eta_{ij} + d_j)^2]^{1/2}}{(\eta_{ij} - d_j) + [(\xi_{ij} + d_j)^2 + (\eta_{ij} - d_j)^2]^{1/2}} \right) \right. \\ & + (\eta_{ij} + d_j) \ln \left(\frac{(\xi_{ij} + d_j) + [(\eta_{ij} + d_j)^2 + (\xi_{ij} + d_j)^2]^{1/2}}{(\xi_{ij} - d_j) + [(\xi_{ij} - d_j)^2 + (\eta_{ij} + d_j)^2]^{1/2}} \right) \\ & + (\xi_{ij} - d_j) \ln \left(\frac{(\eta_{ij} - d_j) + [(\xi_{ij} - d_j)^2 + (\eta_{ij} - d_j)^2]^{1/2}}{(\eta_{ij} + d_j) + [(\xi_{ij} - d_j)^2 + (\eta_{ij} + d_j)^2]^{1/2}} \right) \\ & \left. + (\eta_{ij} - d_j) \ln \left(\frac{(\xi_{ij} - d_j) + [(\xi_{ij} - d_j)^2 + (\eta_{ij} - d_j)^2]^{1/2}}{(\xi_{ij} + d_j) + [(\xi_{ij} - d_j)^2 + (\eta_{ij} - d_j)^2]^{1/2}} \right) \right\} \end{aligned} \tag{5}$$

and

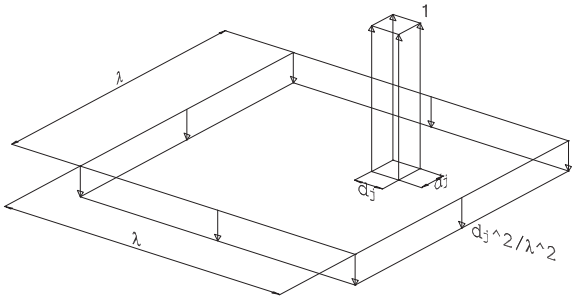

Fig. 2. The self-balanced load on the elementary cell utilized to evaluate the elastic response matrix L_{ij}.

$$l_m = \frac{1-\nu^2}{\pi E}\left(\frac{d_j}{\lambda}\right)^2 \sum_{k=-\infty}^{+\infty}\sum_{h=-\infty}^{+\infty} \times \left\{ \lambda(h+1)\ln\left(\frac{k+1+[(h+1)^2+(k+1)^2]^{1/2}}{k-1+[(h+1)^2+(k-1)^2]^{1/2}}\right) + \lambda(k+1)\ln\left(\frac{h+1+[(k+1)^2+(h+1)^2]^{1/2}}{h-1+[(k+1)^2+(h-1)^2]^{1/2}}\right) + \lambda(h-1)\ln\left(\frac{k-1+[(h-1)^2+(k-1)^2]^{1/2}}{k+1+[(h-1)^2+(k+1)^2]^{1/2}}\right) + \lambda(k-1)\ln\left(\frac{h-1+[(k-1)^2+(h-1)^2]^{1/2}}{h+1+[(k-1)^2+(h+1)^2]^{1/2}}\right)\right\} \quad (6)$$

where d_j is the size of the elementary square cell and $\xi_{ij} = |x_j - x_i| + \lambda h$ and $\eta_{ij} = |y_j - y_i| + \lambda k$.

Eq. (4) can be used to calculate the stress at the interface if the displacements v_i are known. However, our problem belongs to the class of mixed boundary problems since only partial contact conditions occur at the interface: the real contact area is to be determined. Therefore, the solution is sought by means of an iterative incremental procedure: (i) fix the displacement Δ_i, (ii) estimate the contact area as the intersection between the deformed elastic layer, evaluated with respect to the elastic solution found previously for the penetration $\Delta_{i-1} < \Delta_i$, and the rigid rough surface, (iii) calculate the displacements in the contact areas as $v_i = h_i - h_{\max} + \Delta$, where $h_i = h(\mathbf{x}_i)$, $h_{\max}$ the maximum height of the rough profile, (iv) solve Eq. (4) to calculate the stress distribution σ_j in the contact areas, (v) calculate the displacements $v_i = L_{ij}\sigma_j$ out of the contact areas, (vi) update the contact area at every step by eliminating the elements with negative pressure and adding those for which there is penetration.

Note that the inversion of the matrix L_{ij} is done only for those points which belongs to the contact areas, this allows to strongly reduce the computational effort. To invert Eq. (4) we use an iterative method based on a Gauss–Seidel scheme.

About the discretization of the domain D, the classic method (see, for example, Borri Brunetto et al., 2001) produces a base uniform grid where $N \times N$ square elements are always allocated in memory. Such a type of mesh needs allocation of informations concerning also elements not in contact. Wriggers (2002) suggested an alternative method of meshing process using an adaptive uniform grid to allocate only elements in contact to obtain memory saving. By following the approach developed by Carbone and Mangialardi (2008) and Carbone et al. (2009) for the case of 1D contacts, we improve Wriggers' methodology by introducing a non uniform adaptive mesh with a coarse mesh in the inner part of each contact area and a fine mesh where the gradients of the stress and strain quantities are larger (*i.e.* at the borders of the contact clusters). Indeed, this procedure, which we could liken to the spatial search described in Williams and O'Connor (1999) and Wriggers (2002), is based on pure geometric criteria and consists of discretizing the contact areas with the smallest step size at the border and with a following coarsening (with a fixed scale factor 2) as we move toward the inner part of each contact spot. In particular, the smallest step is much smaller than the shortest wavelength of the rigid rough substrate. Specifically, its size has been selected by means of a numerical analysis of convergence which has shown that, for a rough self-affine surface with the shortest wavelength equal to λ, the numerical converged solution is guaranteed by choosing the smallest step size equal to $\lambda/32$.

To point out the computational advances entailed by this method, Fig. 3 shows the number of elements of discretization of the domain D in terms of the imposed penetration Δ for a self-affine fractal surface with Hurst coefficient $H = 0.8$, root mean square roughness $\langle h^2\rangle^{1/2} = 13$ μm, $q_0 = 2\pi \times 10^2$ and $N = 128$. The comparison between the different methods of discretization

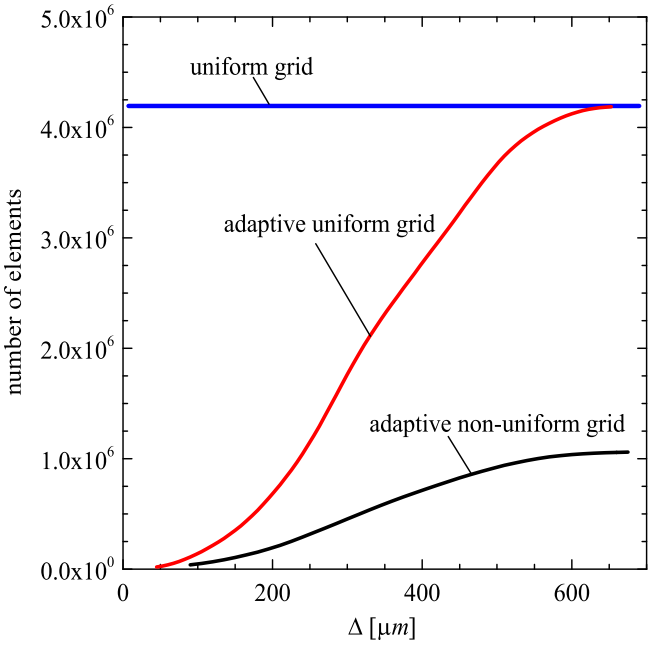

Fig. 3. Number of elements of discretization of the domain D in terms of the imposed penetration Δ, for a self-affine fractal surface with Hurst coefficient $H = 0.8$, root mean square roughness 13 μm, $q_0 = 2\pi \times 10^2$ and $N = 128$. Comparison between different methods of discretization: uniform grid, adaptive uniform grid and adaptive non-uniform grid.

(uniform grid, adaptive uniform grid and adaptive non-uniform grid) makes clear that the total number of elements significantly reduces by employing the procedure we propose, with a great benefit in terms of computational costs. For example, with a penetration $\Delta = 400$ μm the cells allocated in memory are about 7×10^5. Such number would be 2.75×10^6 with an adaptive uniform mesh and 4.2×10^6 with a classical uniform grid.

3. Results

All calculations have been performed assuming that half-space is linearly elastic with Young's modulus $E = 0.4$ GPa and Poisson's

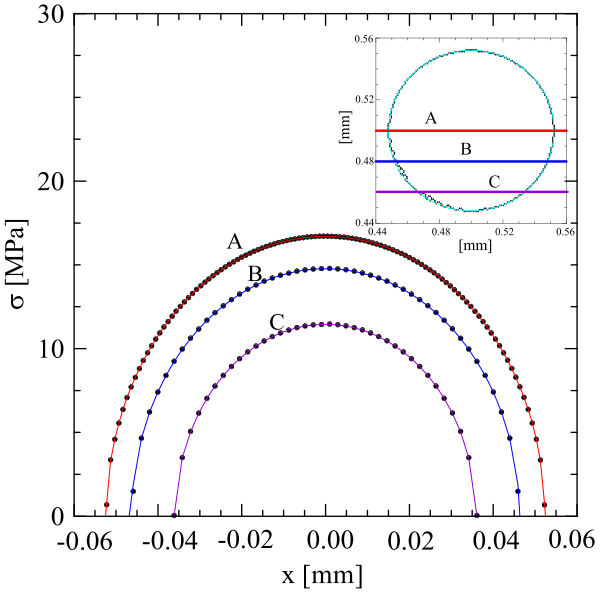

Fig. 4. Contact area and pressure distribution for an elastic half-space indented by a rigid sphere of radius $R = 10^{-2}$ m: comparison between numerical and analytical results obtained for an imposed displacement $\Delta = 25$ μm.

ratio $\nu = 0.45$. For each surface we have considered seven different realizations and taken the averaged results. Also, the numerical convergence of the proposed method has been verified by comparing the numerical results with the Hertzian solution and by checking the trend of the stress probability distribution at the interface which must vanish as the interfacial stress σ goes to zero (Persson et al., 2002; Persson, 2006; Manners and Greenwood, 2006).

Fig. 4 shows a comparison between the circular contact area predicted by the analytical Hertzian solution and the present numerical approach, for the case of a rigid sphere of radius $R = 10^{-2}$ m indenting an elastic half-space. Results are obtained for an imposed displacement $\Delta = 25$ μm. In particular, for the three sections shown in Fig. 4, we have also compared the Hertzian pressure distribution (solid lines) with the numerical one (circular dots), obtaining a very good agreement.

However our aim is to investigate the contact between a rough surface and a linear elastic half-space. For a fractal surface generated by spectral methods, and characterized by a Hurst coefficient $H = 0.8$, a root mean square roughness 13 μm, long wave length roll-off vector $q_0 = 2\pi \times 10^2$ and two different values of number of wavelengths $N = 64{,}128$, Fig. 5 shows the real contact area normalized with respect to the nominal one A/A_0 as a function of the dimensionless average contact pressure σ_0/E^* (being $E^* = E/(1-\nu^2)$ the composite Young's modulus). Red dots are for $N = 64$ and blue triangles are for $N = 128$. Also a linear interpolation of numerical data is plotted. The relation between the contact area and the applied load is clearly linear, according to some analytical theories (Persson, 2001) and other numerical investigations (Yang et al., 2006; Hyun et al., 2004; Carbone and Bottiglione, 2008; Campana and Muser, 2007). However the slope of the linear relation is affected by the number of wavelengths which the rough surface is constituted of. The reason for such a behavior is that increasing the number of wavelengths of the surface PSD, the number of asperities of the surface strongly increases and also their size decreases, the contact is then split in smaller and smaller parts and in the limit of an endless number of wavelengths the contact area would actually vanish. This is clearly shown in Fig. 6, where, assuming an external applied dimensionless load $\sigma_0/E^* = 8.9 \times 10^{-4}$, the contact area corresponding to $N = 64$ (Fig. 5a) is larger and less jagged than for $N = 128$ (Fig. 5b).

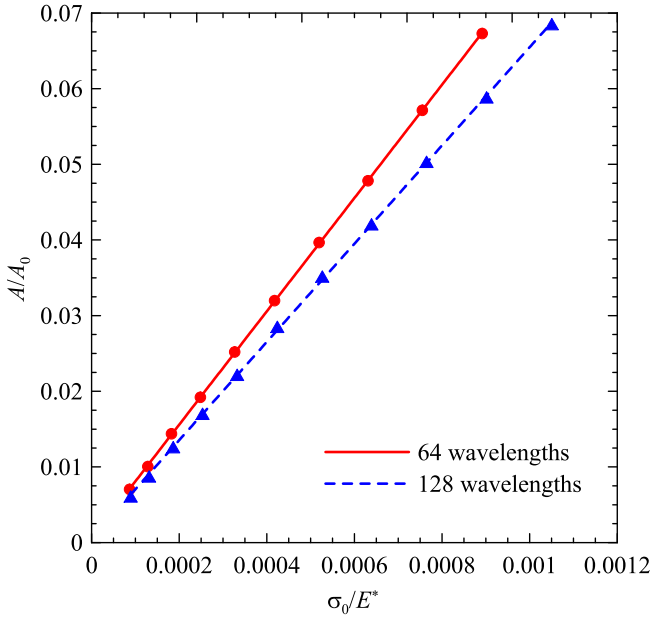

Fig. 5. Variation of the real contact area A normalized with respect to the nominal one A_0 with the dimensionless average contact pressure σ_0/E^*, for 64 (red dots) and 128 (blue triangles) wavelengths of the power spectral density of the generated self-affine fractal surface. Solid and dashed lines are linear interpolation of numerical data (coefficient of determination $R^2 > 0.9999$). (For interpretation of the references to colour in this figure legend, the reader is referred to the web version of this article.)

The variation of the dimensionless load σ_0/E^* with the dimensionless penetration Δ/h_{max} is instead shown in Fig. 7 in a linear-log plot. We observe that except for small Δ values, the relation between the quantity $\log_{10}(\sigma_0/E^*)$ and the penetration Δ is linear. This is in agreement with some molecular dynamics calculations (Yang and Persson, 2008) and also in good agreement with experiments (Lorenz and Persson, 2009; Lorenz et al., 2010). However at small indentations, this behavior is lost because we are working with a finite system, and a finite system has asperities with height below some finite value h_{max}, so that when the distance between the half-space and the mean plane of the rough surface is larger than h_{max} no contact can occur between the solids. As a consequence the quantity $\log_{10}(\sigma_0/E^*)$ must more than linearly decrease as Δ approaches zero. On the other hand for infinite systems linearity should hold true even when the distance between the elastic half-space and rough surface is very large. The reason is simply that infinitely large rough surfaces have an infinite number of asperities with arbitrary height.

It is also worth to notice that the relation between the dimensionless load σ_0/E^* and Δin Fig. 7 is only marginally affected by the number of wavelengths included in the surface PSD provided that the roll-off wave vector q_0 remains unchanged. This result is in agreement with some theoretical predictions (Persson, 2001), numerical simulations (Yang and Persson, 2008) and some experiments (Lorenz et al., 2010). In particular, the indentation is strongly influenced by the surface rms roughness h_{rms} which is only negligible affected by the short wavelength component of the PSD of the rough substrate (Yang and Persson, 2008). Therefore, including more high-frequency terms does not involve a change of the indentation. In other words, an increase of the number of wavelength N only induces a strong decrease of the real contact area but does not significantly modify the mid-low frequency content of the deformed surface; hence, for fixed applied load, the strain energy stored at the interface does not change significantly with N (Yang et al., 2006) leading to the observed insensitivity of the indentation to high frequency content of the surface PSD.

Now, we will focus on the probability distribution of the interfacial normal stress. The full stress probability distribution $P_f(\sigma)$ is equal to $P_f(\sigma) = \frac{A_0 - A}{A_0}\delta(\sigma) + \frac{A}{A_0}p(\sigma)$, where $\delta(\sigma)$ is the δ-peak at $\sigma = 0$, related to the size of the non-contact area, and the distribution $p(\sigma)$ is the probability density function in the contact area. In Fig. 8, we show the stress probability function $P(\sigma) = \frac{A}{A_0}p(\sigma)$: Red dots corresponds to numerical predictions, whereas solid and dashed lines to the best fit obtained by a double Gaussian distribution, according to (Persson, 2001)

$$P(\sigma) = \frac{1}{2(\pi\Lambda)^{1/2}}\left[e^{-(\sigma-\sigma_0)^2/(4\Lambda)} - e^{-(\sigma+\sigma_0)^2/(4\Lambda)}\right] \tag{7}$$

where Λ is the fitting parameter. The numerically calculated trend of $P(\sigma)$ correctly decreases linearly to zero as σ is decreased. This is a very crucial point, since Persson et al. (2002), Persson (2006) and Manners and Greenwood (2006) have shown analytically that this behavior of $P(\sigma)$ must necessarily be observed. It is worth noticing that other calculations (Hyun and Robbins, 2007; Hyun et al., 2004; Luan et al., 2006; Campana et al., 2008; Cheng and Robbins, 2010) do not present this trend. The reason for that is due, in our opinion, to the insufficient mesh refinement at the border of the contacts, or to the insufficient number of mesh points in each contact spot (in case of uniform grid), which is a common problem also in FEM approaches. Indeed, Campana and Muser (2007) have shown, by employing the so-called Green's function molecular dynamics, that

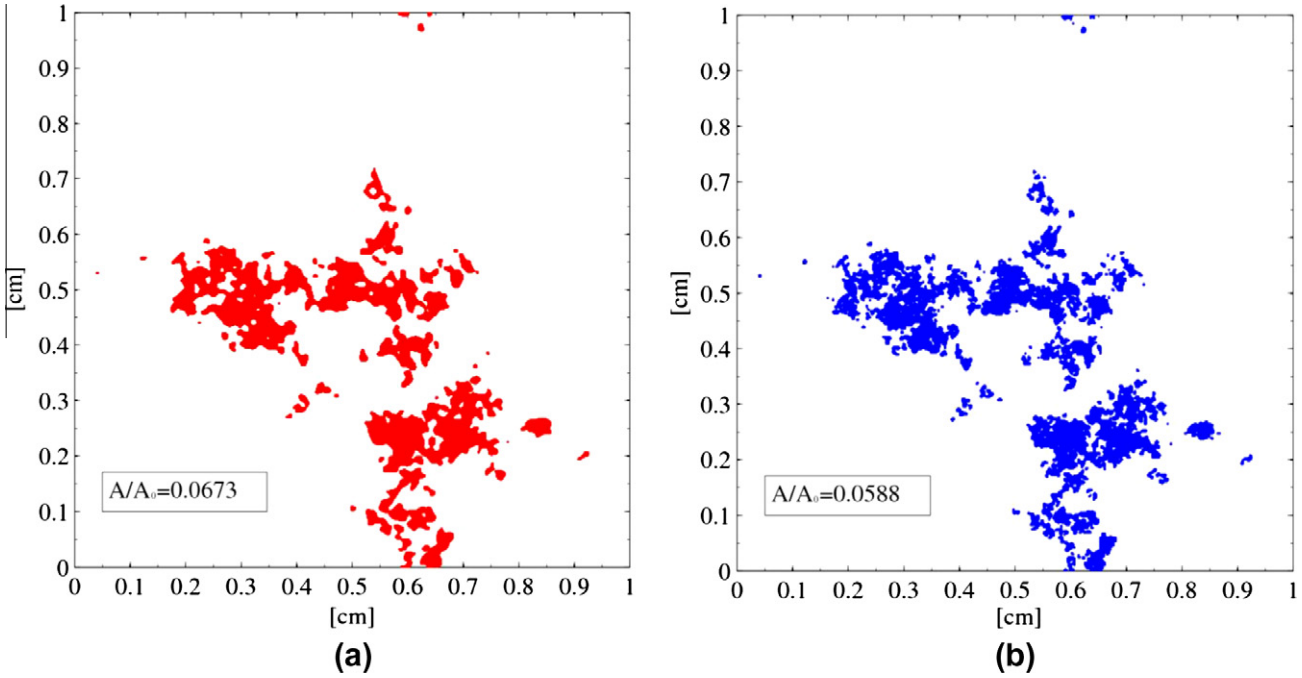

Fig. 6. Distribution of the contact spots for $\sigma_0/E^* = 8.9 \times 10^{-4}$: (a) effective contact region for a power spectral density of the generated self-affine fractal surface with 64 wavelengths ($A/A_0 = 0.0673$); (b) effective contact region for a power spectral density of the generated self-affine fractal surface with 128 wavelengths ($A/A_0 = 0.0588$).

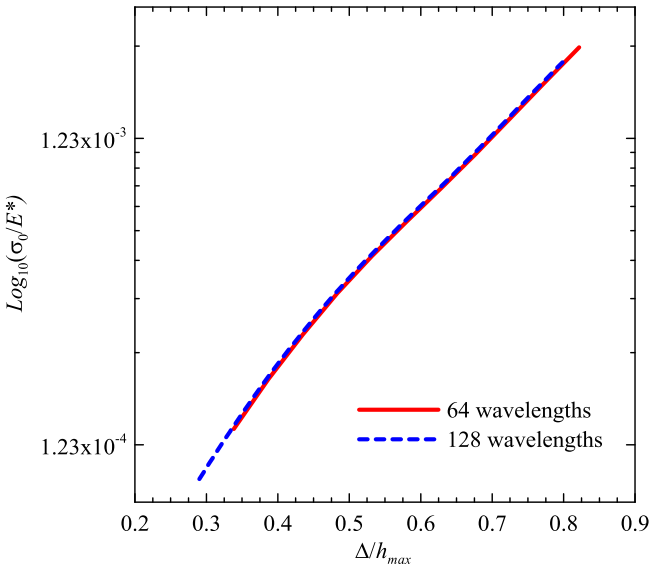

Fig. 7. Variation of the dimensionless load σ_0/E^* with the dimensionless penetration Δ/h_{max} for 64 (solid line) and 128 (dashed line) wavelengths of the power spectral density of the generated self-affine fractal surface.

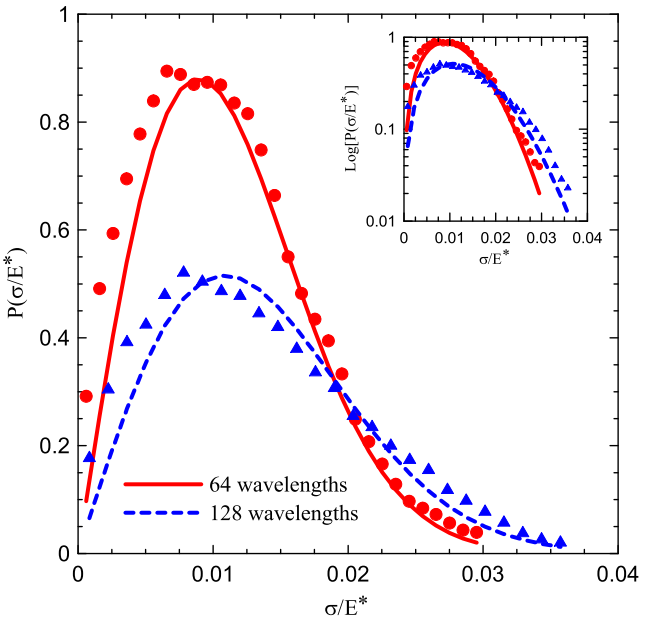

Fig. 8. Stress probability distribution $P(\sigma/E^*)$ of the dimensionless interfacial normal stress distribution σ/E^*: Red dots corresponds to numerical results, solid and dashed lines corresponds to the best fit obtained by Eq. (7). (For interpretation of the references to colour in this figure legend, the reader is referred to the web version of this article.)

a non-sufficiently fine mesh provokes a distorted solution and prevents the stress probability distribution from vanishing linearly with decreasing σ.

Moreover, the inset of Fig. 8 shows the same data in a semi-logarithmic scale. The parabolic shape of stress probability distribution, observed at larger stresses, demonstrates that the tail of $P(\sigma)$ is really Gaussian. Furthermore Fig. 8 shows that increasing the number N of wavelengths the stress probability distribution spreads towards higher values of stress σ. Of course, the observed decrease, for fixed load, of the contact area as N is increased (see Fig. 5), explains the reduction of the integral $\int_0^\infty P(\sigma)d\sigma = A/A_0$ as N raises.

4. Conclusion

In this work we have developed a new efficient numerical method to determine the contact area, the stress distribution, the penetration and elastic deformation of a periodic numerically generated self-affine fractal rigid surface and a linear elastic half-space. The method is based on a Green's function approach and employs an original non uniform adaptive mesh, which gives a great benefit, in terms of computational costs, to determine the

solution of the problem. The numerical convergence has been verified by comparing the numerical results with the Hertzian solution.

Results show the existence of a linear relation between the contact area and the applied load and an exponential dependence of the external applied stress on the separation between the two approaching surfaces. We also observe that the contact area reduces as the number N of wave components of the rough surface is increased. Furthermore, the stress probability distribution of the interfacial normal stress has also been calculated. We show that, at small stresses, it linearly decreases to zero. This results indirectly confirms that our numerical method is able to get converged results even in the case of contact between randomly rough surfaces, which involve a very large number of very small contact spots.

Appendix A. Generation of a self-affine randomly rough surface

In order to carry out the numerical simulations and compare the results with the theoretical predictions, we need to numerically generate the rough surface. We have opted for a fractal self-affine isotropic geometry. For any self-affine fractal surface $h(\mathbf{x})$ the statistical properties are invariant under the transformation

$$\mathbf{x} \to t\mathbf{x}; \quad h \to t^H h \tag{8}$$

in such a case it can be shown that for isotropic surface the PSD is

$$C(q) = C_0 \left(\frac{q}{q_0}\right)^{-2(H+1)} \tag{9}$$

where $q = |\mathbf{q}|$, H is the Hurst exponent of the randomly rough profile, which is related to the fractal dimension $D_f = 3 - H$. In order to carry out the numerical calculations we have utilized a periodic surface with Fourier components up to the value $q_1 = Nq_0$. The representation of such a surface in exponential form is then

$$h(\mathbf{x}) = \sum_{hk=-\infty}^{+\infty} a_{hk} \exp(i\mathbf{q}_{kh} \cdot \mathbf{x}) \tag{10}$$

where $\mathbf{q}_{kh} = (kq_0, hq_0), \mathbf{x} = (x,y)$. Since $h(\mathbf{x})$ is real we must have $a_{-h,-k} = \overline{a_{hk}}$. Moreover for randomly rough surface the following relation must be satisfied $\langle a_{hk} a_{lm} \rangle = 0$ with $l \neq -h$, $m \neq -k$, where the symbol $\langle \dots \rangle$ is the ensemble average operator. Now we can calculate the PSD of surface Eq. (10)

$$C(\mathbf{q}) = \sum_{hk=-\infty}^{+\infty} \langle |a_{hk}|^2 \rangle \delta(\mathbf{q} - \mathbf{q}_{hk}) \tag{11}$$

from which it follows

$$C(\mathbf{q}_{hk}) = \langle |a_{hk}|^2 \rangle \delta(\mathbf{0}) \tag{12}$$

For isotropic surfaces we have $C(\mathbf{q}) = C(q)$ which simply gives $C(\mathbf{q}_{hk}) = C(q_0\sqrt{h^2+k^2})$ and assuming self-affine fractal surface [see Eq. (9)] one obtains

$$\langle |a_{hk}|^2 \rangle = \langle |a_{11}|^2 \rangle \left(\frac{h^2+k^2}{2}\right)^{-H-1} \tag{13}$$

Hence the quantities $\langle |a_{hk}|^2 \rangle$ can be determined once known $\langle |a_{11}|^2 \rangle$ and the Hurst exponent of the fractal surface. However to completely characterize the rough profile we still need the probability distribution of the quantities a_{hk}. We first observe that the condition $\langle a_{hk} a_{lm} \rangle = 0$ with $l \neq -h$, $m \neq -k$ is satisfied if the phases φ_{hk} of the complex quantities a_{hk} are random numbers uniformly distributed between 0 and 2π. We also recall the condition $a_{-h,-k} = \overline{a_{hk}}$ also implies that $|a_{-h,-k}| = |a_{h,k}|$ and that the quantities $\varphi_{-h\,-\,k} = -\varphi_{hk}$. So what we need now is only the probability distribution of $|a_{h,k}|$. Of course there are several choices and the simplest one is to assume that the probability density function of $|a_{hk}|$ is just a Dirac's delta function centered at $\langle |a_{hk}|^2 \rangle^{1/2}$, i.e.

$$P(|a_{hk}|) = \delta(|a_{hk}| - \langle |a_{hk}|^2 \rangle^{1/2}) \tag{14}$$

It can be shown (Persson et al., 2005) that this choice guarantees also that the random profile $h(\mathbf{x})$ has a Gaussian random distribution. Several other spectral methods are well known in literature: for details we refer to Dieker and Mandjes (2003).

References

Borri Brunetto, M., Chiaia, B., Ciavarella, M., 2001. Incipient sliding of rough surfaces in contact: a multi-scale numerical analysis. Comput. Methods Appl. Mech. Eng. 190, 6053–6073.

Campana, C., Muser, M.H., 2007. Contact mechanics of real vs. randomly rough surfaces: A Green's function molecular dynamics study. Europhys. Lett. 77 (3), 38005.

Campana, C., Muser, M., Robbins, M.O., 2008. Elastic contact between self-affine surfaces: comparison of numerical stress and contact correlation functions with analytic predictions. J. Phys. Condensed Matter. 20, 354013.

Carbone, G., Mangialardi, L., 2004. Adhesion and friction of an elastic half-space in contact with a slightly wavy rigid surface. J. Mech. Phys. Solids 52 (6), 1267–1287.

Carbone, G., Mangialardi, L., 2008. Analysis of the adhesive contact of confined layers by using a Green's function approach. J. Mech. Phys. Solids 56, 684–706.

Carbone, G., Bottiglione, F., 2008. Asperity contact theories: Do they predict linearity between contact area and load? J. Mech. Phys. Solids 56, 2555–2572.

Carbone, G., Scaraggi, M., Tartaglino, U., 2009. Adhesive contact of rough surfaces: Comparison between numerical calculations and analytical theories. Eur. Phys. J. E 30 (1), 65–74.

Cheng, S., Robbins, M.O., 2010. Defining contact at the atomic scale. Tribol. Lett. 39, 329–348.

Dieker, A.B., Mandjes, M., 2003. On spectral simulation of fractional Brownian motion. Probab. Eng. Inform. Sci. 17, 417–434.

Geim, A.K., Dubonos, S.V., Gricorieva, I.V., Novoselov, K.S., Zhukov, A.A., Shapoval, S.Yu., 2003. Microfabricated adhesive mimicking gecko foot-hair. Nat. Mater. 2, 461–463.

Greenwood, J.A., Williamson, J.B.P., 1966. Contact of nominally flat surfaces. Proc. R. Soc. Lond. A. 295, 300–319.

Greenwood, J.A., 2006. A simplified elliptic model of rough surface contact. Wear 261, 191–200.

Greenwood, J.A., Putignano, C., Ciavarella, M., 2011. A Greenwood & Williamson theory for line contact. Wear 270, 332–334.

Hyun, S., Pei, L., Molinari, J.-F., Robbins, M.O., 2004. Finite-element analysis of contact between elastic self-affine surfaces. Phys. Rev. E 70, 026117.

Hyun, S., Robbins, M.O., 2007. Elastic contact between rough surfaces: Effect of roughnessat large and small wavelengths. Tribol. Int. 40, 413–1422.

Johnson, K.L.J., 1985. Contact Mechanics. Cambridge University Press.

Lorenz, B., Persson, B.N.J., 2009. Interfacial separation between elastic solids with randomly rough surfaces: comparison of experiment with theory. J. Phys.: Condens. Matter. 21 (1), 015003.

Lorenz, B., Carbone, G., Schulze, C., 2010. Average Separation between solids in rough contact: comparison between theoretical predictions and experiments. Wear 268 (7-8), 984–990.

Luan, B.Q., Hyun, S., Molinari, J.F., Bernstein, N., Robbins, M.O., 2006. Multiscale modeling of two-dimensional contacts. Phys. Rev. E 74, 046710.

Manners, W., Greenwood, J.A., 2006. Some observations on Persson's diffusion theory of elastic contact. Wear 261, 600–610.

Persson, B.N.J., 2001. Theory of rubber friction and contact mechanics. J. Chem. Phys. 115, 3840–3861.

Persson, B.N.J., Albohr, O., Tartaglino, U., Volokitin, A.I., Tosatti, E., 2005. On the nature of surface roughness with application to contact mechanics, sealing, rubber friction and adhesion. J. Phys.: Condens. Matter. 17, 1–62.

Persson, B.N.J., Bucher, F., Chiaia, B., 2002. Elastic contact between randomly rough surfaces: comparison of theory with numerical results. Phys. Rev. B 65, 184106.

Persson, B.N.J., 2006. Contact mechanics for randomly rough surfaces. Surface Science Reports 61, pp. 201–227.

Sundararajan, S., Bhushan, B., 2001. Static friction and surface roughness studies of surface micromachined electrostatic micromotors using an atomic force friction force microscope. J. Vacuum Sci. Technol. A 19 (4), 1777–1785.

Williams, J.R., O'Connor, R., 1999. Discrete element simulation and the contact problem. Arch. Comput. Methods Eng. 6 (4), 279–304.

Wriggers, P., 2002. Computational Contact Mechanics. Wiley& Sons Ltd, Chichester.

Yang, C., Tartaglino, U., Persson, B.N.J., 2006. A multiscale molecular dynamics approach to contact mechanics. Eur. Phys. J. E Soft-Matter. 19 (1), 47–58.

Yang, C., Persson, B.N.J., 2008. Molecular dynamics study of contact mechanics: contact area and interfacial separation from small to full contact. Phys. Rev. Lett. 100, 024303.